

Adaptive Subband Compression of Streaming Data for Power System Monitoring and Control

Xinyi Wang, Yilu Liu, and Lang Tong

Abstract—A data compression system capable of providing high-fidelity high-resolution streaming of power system real-time measurements is proposed. Referred to as adaptive subband compression, the proposed technique partitions the signal space into subbands and adaptively compresses subband signals based on each subband’s active bandwidth. The proposed technique conforms to existing industry phasor measurement standards. It applies to the streaming of phasor measurements or high-frequency point-on-wave samples of power system signals. Experiments on synthetic and real data show that the proposed technique reduces the required communication data rate by several orders of magnitude while maintaining the precision required by the industry standards.

Index Terms—Phasor measurement unit (PMU), point-on-wave (POW) measurement, power system monitoring and control, subband coding, adaptive data compression.

I. INTRODUCTION

The phasor measurement unit (PMU) technology invented in the late ’80s was considered a breakthrough in power systems monitoring and control. By communicating synchronized phasor and frequency measurements at the rate of 60 to 120 measurements per second to the control center, the PMU technology has the potential to revolutionize power system operations by providing fast-timescale situational awareness and enhanced network resilience [1].

Despite the substantial investments worldwide, the full potential of the PMU technology has yet been realized. A reason for this underachievement is that PMUs need to be broadly deployed to be effective. The current level of PMU installation remains limited, however, sufficient for some high voltage networks but inadequate for large systems. The limited PMU presence results in the lack of demonstrated “killer applications” that inhibits the necessary investments for wider deployments.

With deeper penetration of inverter-based resources that exhibit low inertia and fast dynamics, there are compelling needs for an ultra-high-rate grid measurement technology that provides a kilohertz-level high-resolution data streaming [2]. Such technology has the potential to enable in-situ transient stability assessments and wide-area real-time control.

Xinyi Wang and Lang Tong ({xw555,lt35}@cornell.edu) are with the School of Electrical and Computer Engineering, Cornell University, USA. Yilu Liu (liu@utk.edu) is with the Department of Electrical and Engineering and Computer Science, The University of Tennessee, Knoxville. This work was supported in part by the National Science Foundation under Grants 1932501 and 1816397

A major barrier for the streaming of ultra-high-rate measurements is the network bandwidth required. A direct implementation of high-resolution data streaming would require up to ten to one hundred-fold increases of required network bandwidth. To this end, an enabling technology for high-resolution data streaming is data compression that delivers high-fidelity and high-resolution measurements subject to bandwidth constraints of the existing infrastructure.

A back-of-the-envelope calculation gives an estimate of the level of compression required to stream high-resolution data under current communication constraints. The current IEEE standards for PMU [3], [4] recommend that PMU measurements include the possibility of harmonics up to the 50th order, which implies that the maximum bandwidth of the original (source) signal is approximately 3 (kHz). By the Nyquist sampling theorem, the signal should be sampled at 6 (kHz) to achieve perfect reconstruction. If the standard PMU reporting frame rate of 60 samples per second is used for streaming PMU data, a 100 to 1 compression ratio would be required. A higher compression ratio is necessary if the analysis of high-resolution transient signals is needed. The existing technologies do not come close to this level of compression. See [5].

Having a high degree of compression is only one metric of consideration. Fundamental to the compression of streaming data is a tradeoff among three factors: (i) the compression ratio, (ii) the accuracy of the reconstruction of the source from the compressed data, and (iii) the delay associated with the compression and decompression processes. The first two were formalized in an information-theoretic setting as the rate-distortion tradeoff by Shannon [6]. The last is particularly relevant to streaming applications in which encoding and decoding delays are significant design constraints.

A. Related Literature

The need for data compression for power system monitoring goes back at least three decades. Mehta and Russell made one of the earliest contributions in [7], where the authors articulated the compression needs. They recommended compressing data in the frequency domain by discarding high-frequency coefficients via Fast Fourier Transform (FFT).

Discarding high-frequency components may lead to significant distortions when the signal has higher-order harmonics. Nonetheless, a modification of Mehta and Russell’s sugges-

tion by a reverse water-filling strategy can achieve the optimal tradeoff between compression ratio and reconstruction error for Gaussian processes [8]. The caveat for the FFT-based compression optimality is that the FFT block size must be arbitrarily large, which conflicts with the low latency requirement of data streaming. When the FFT block size is limited to reduce encoding-decoding latency, the FFT-based compression introduces inter-block distortions, resulting in the loss of signal details and high reconstruction errors.

There is an extensive literature in data compression for power quality data at digital fault recorders (DFR) [9]–[14]. For such applications, the data sampling rate can be as high as 10MHz. Because the recorded data are only uploaded on-demand, often in post-event analysis, data must be communicated in high accuracy. Thus lossless compression techniques are usually preferred. Block linear processing techniques such as FFT, discrete-cosine transform (DCT), wavelet/spline have been developed [7], [9]–[16]. Nonlinear techniques such as neural network, fuzzy logic, and principal component analysis (PCA) have also been proposed [12], [15], [17], [18].

The literature on the compression of streaming data for power system monitoring and control is limited. See a survey on compression techniques for smart grid operations [5], where the authors reported the capabilities of various compression techniques with the compression ratio up to 5:1 for lossless compressions. Most relevant to our work are the lossy compressions, categorized by wavelet (and waveform packet) transform techniques, mixed transform, and parametric compression techniques. These state-of-the-art methods offer a 6 to 16:1 compression ratio at the normalized mean squared error (NMSE) from -20 to -30 dB.

In a broader context, the idea of subband compression considered in this paper has long been successfully applied in multimedia communications. Most of the data-streaming techniques (such as the H.264 group) employ some forms of subband compression. The key to subband compression is to exploit the signal’s subband properties to apply high levels of compression in subbands where artifacts of compression are the least significant. For instance, in audio and video compression, the audio/video signals’ perceptual properties play a crucial role in achieving tradeoffs among compression ratio, reconstruction accuracy, and encoding-decoding latency. In this paper, we focus on exploiting the harmonic structure of the power signal for compression.

B. Summary of Results and Contributions

We propose a lossy compression technique for the *high-fidelity and high-resolution* data streaming of measurements for wide-area monitoring and control. By high-fidelity, we mean that the signal reconstruction has a low mean-squared error within the specification of industry standards. On the other hand, by high-resolution, we mean that the source signal is sampled at a high frequency to include higher-order harmonics, wideband interharmonics, and wideband transient

signals. Our goal is to achieve a 100:1 to 1000:1 compression ratio with a reconstruction accuracy satisfying the industrial standards [3], [4]. The proposed technique applies to the streaming of PMU as well as high-resolution point-on-wave (POW) measurements.

The proposed technique is referred to as *adaptive sub-band compression (ASBC)* that compresses measurements adaptively based on a subband decomposition of the signal spectrum. ASBC can operate in dual modes. One mode is for monitoring and control in which PMU or POW measurements are streamed to the control center with a relatively small delay. The other is for real-time signal analysis (*e.g.*, during contingency events) when the control center requires higher-resolution details in specific harmonic and interharmonic subbands.

Fig. 1 illustrates a conceptual infrastructure realization of the ASBC technology. ASBC consists of an encoder for each remote sensing device and a decoder at the fusion center¹. Together, they form the ASBC codec that provides end-to-end data streaming. Implementations of the ASBC codec are explained in Sec. III-IV.

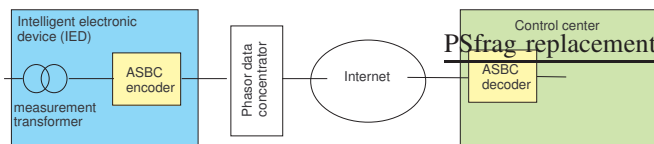


Fig. 1. An application of ASBC technology for high resolution PMU monitoring of power grids.

ASBC partitions the power signal spectrum into harmonic and interharmonic subbands. The harmonic subbands are centered at integral multiples of the system frequency (50 or 60 Hz). Each harmonic subband contains frequency components within the sideband of a specific bandwidth. The interharmonic subband, on the other hand, is a set of frequency bands between harmonic subbands [19].

To achieve a high compression ratio without compromising accuracy, ASBC compresses subband signals adaptively in both time and frequency domains. The encoder monitors the activity levels of subbands and transmits only signals from active subbands. Such an approach is especially useful when some of the subbands are transient. For example, the interharmonic signals are often episodic and wideband. The level of interharmonics may be negligible most of the time and becomes strong suddenly when magnified by resonance. Thus an in-situ compression of interharmonics can achieve a high compression ratio without affecting reconstruction accuracy.

¹A fusion center is a location where data streams from different sensing devices are combined. A fusion center may be located at PMU data concentrators (PDC) or the operator’s control center.

II. SIGNAL MODEL AND SUBBAND DECOMPOSITION

We model the continuous-time voltage (or current) signal $x(t)$ as the sum of harmonics $x_k(t)$ and interharmonics $e(t)$:

$$x(t) = x_0(t) + \sum_{k=1}^K x_k(t) + e(t), \quad (1a)$$

$$x_k(t) = a_k(t) \cos((k+1)\Omega_0 t + \phi_k(t)), \quad (1b)$$

where $x_0(t)$ is the signal component associated with the system frequency F_0 (e.g., 50 or 60 Hz), and $\Omega_0 = 2\pi F_0$. Here we allow $x_0(t)$ and its harmonics $x_k(t)$ to take the general analytical form of (1b). The interharmonic $e(t)$ also models measurement noise outside the harmonic subbands.

Let $X(f)$, $X_k(f)$ and $E(f)$ be the Fourier spectra² of $x(t)$, $x_k(t)$, and $e(t)$, respectively, as illustrated in Fig. 2. We assume that the spectrum $X_k(f)$ of the k th harmonic $x_k(t)$ is centered around $(k+1)F_0$ with passband bandwidth³ of $W_k < F_0$. The total bandwidth of $x(t)$ is therefore $KF_0 + \frac{W_k}{2} \leq (K + \frac{1}{2})F_0$.

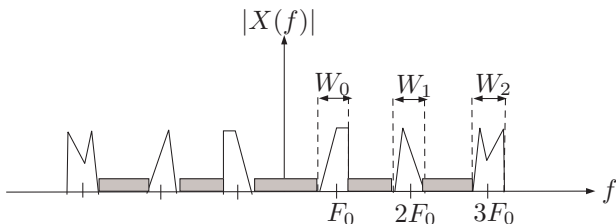


Fig. 2. The spectrum of $x(t)$ and its harmonics. The grey area represents the spectrum of interharmonics.

Sampled at the frequency of $F_s = \frac{1}{T_s} \geq (2K+1)F_0$ (Hz), the discrete-time signal is given by, for $n = 0, \pm 1, \dots$,

$$x[n] := x(nT_s) = x_0[n] + \sum_{k=1}^K x_k[n] + e[k], \quad (2a)$$

$$x_k[n] := a_k[n] \cos\left(\left(k+1\right)\frac{\Omega_0}{F_s}n + \phi_k[n]\right), \quad (2b)$$

where $(a_k[n], \phi_k[n])$ are the sampled amplitude and phase angles and $e[n]$ the interharmonic signal.

III. ADAPTIVE SUBBAND COMPRESSION: ENCODER

As part of the remote terminal unit, the ASBC encoder partitions the signal spectrum into a set of frequency bands. It adaptively masks inactive bands and encodes the unmasked bands in parallel. Fig. 3 illustrates the schematic of the ASBC encoder. The functionalities of individual components are explained below.

²Here we assume the existence of Fourier transforms of all signals.

³The *passband bandwidth* is defined by the width of the frequency band containing non zero frequency components.

A. Subband decomposition

From the output of the sensor transformer, the continuous-time measurement signal $x(t)$ is sampled at F_s Hz. The discrete-time signal $x[n]$ is frequency down-shifted and passed through a filterbank $\mathcal{H} = (\mathcal{H}_e, \mathcal{H}_0, \dots, \mathcal{H}_K)$ that extracts the subband signal $x_k[n]$ in its baseband representation $y_k[n]$. Specifically, the output of the k th subband filter is a complex time series

$$y_k[n] = (x[n]e^{-jk\omega_0 n}) \otimes h_k[n], \quad \omega_0 := \frac{2\pi F_0}{F_s},$$

where \otimes is the convolution operator. Ideally, the filter for the k th subband is a low-pass filter with bandwidth $W_k/2$, whose output $y_k[n]$ is the baseband representation of the k th harmonic signal $x_k[n]$, and its continuous-time counterpart is $\tilde{x}_k(t) = x_k(t)e^{-jk\Omega_0 t}$.

The interharmonic distortion $y_e[n]$ whose spectrum corresponds to the grey area of power spectrum in Fig. 2 can be extracted by

$$y_e[n] = x[n] - \sqrt{2}\text{Re}\left(\sum_{k=1}^K y_k[n]e^{jk\omega_0 n}\right).$$

In absence of high order and interharmonics, $x(t) = x_0(t)$ in (1), and only $y_0[n]$ is non-zero.

B. Activity detection

Except $y_0[n]$ from the output of subband filter \mathcal{H}_0 corresponding to the subband associated with the system frequency F_0 , the outputs from the rest of subband filters are passed through activity detectors ($\mathcal{D}_e, \mathcal{D}_k$) to determine the level of compression required, ranging from transmitting at the subband Nyquist rate to full compression that eliminates the transmission of $y_k[n]$.

The activity detection is performed on blocks of samples. The detector \mathcal{D}_k takes a block of samples and outputs an indicator $w_k = 1$ for the block if the subband k is active and $w_k = 0$ otherwise. The detector for inter-harmonic subband does the same way. A standard implementation of the activity detector is the energy detector whereas more sophisticated techniques such as quickest detection or machine-learning based detection can also be used.

C. Subband compression

The compression of the harmonic subband k is achieved by down-sampling of $y_k[n]$ by S_k fold. By the (passband) Nyquist sampling theorem, if the k th subband has passband bandwidth of W_k , then the signal in the k th subband can be perfectly reconstructed by sampling $x_k(t)$ at frequency of W_k (Hz). Given that $x(t)$ is sampled at F_s (Hz), the rate of down-sampling S_k is given by

$$S_k = \left\lceil \frac{F_s}{W_k} \right\rceil.$$

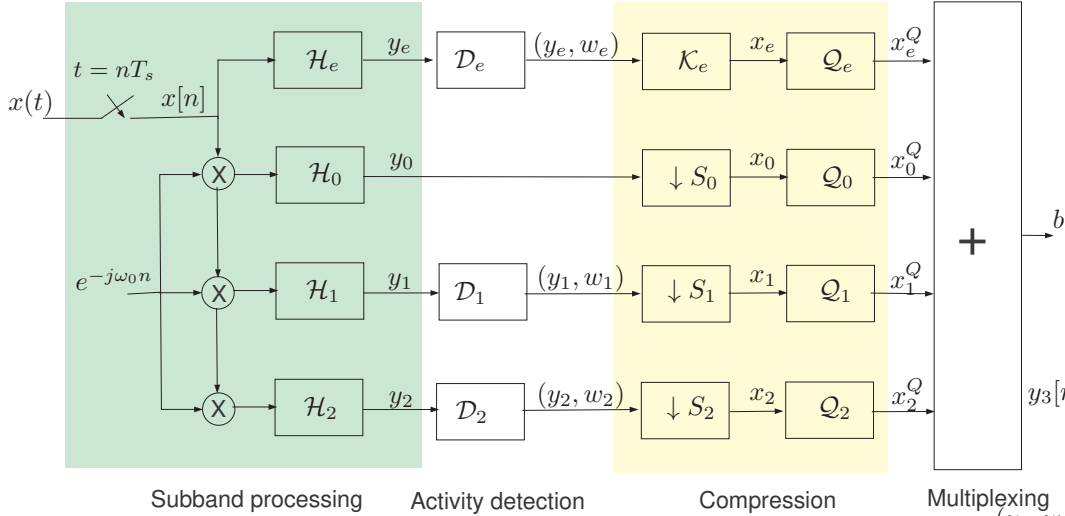


Fig. 3. A three-subband ASBC encoder where $h_k[n]$ is the impulse response of the k th subband filter. Time indices of signals are omitted with y_i standing for sequence $(y_i[n])$.

If subband k is active, the down-sampler gives the compressed data sequence

$$x_k[n] = \begin{cases} y_k[n], & n \equiv 0 \pmod{S_k} \text{ and } w_k[n] = 1, \\ \#, & \text{otherwise,} \end{cases} \quad (3)$$

where $\#$ is a masking symbol indicating that the data sample needs not be encoded and transmitted. Note that, although we define $x[n]$ for all n , only unmasked data blocks are transmitted over the network. The data rate associated with $x_k[n]$ is at most $1/S_k$ of that of $y_k[n]$.

The interharmonic band is expected to be active infrequently. When an interharmonic signal needs to be transmitted to the control center, an FFT-based (e.g., FFT- (k, L)) described in Sec. V-B) or wavelet based compression scheme can be used. See references in [5].

D. Quantization and multiplexing

The down-sampled data streams are quantized by quantizer (Q_e, Q_k) that maps subband stream $x_k[n]$ into a bit-stream x_k^Q of R_k bits/sample. A scalar quantizer such as pulse-code modulation (PCM) quantizes individual sample of x_k into R_k bits of x_k^Q , whereas a vector quantizer such as code excited linear prediction (CLEP) or K-mean clustering takes a block of M samples of and quantizes them into a block of MR_k bits of x_k^Q . The bit-streams from subbands are multiplexed into a single bit-stream b to be delivered to the receiver. Also communicated are the sequences of activity indicators $\#,$ one for each block that is not transmitted due to inactivity.

IV. ADAPTIVE SUBBAND COMPRESSION: DECODER

The ASBC decoder is located at the regional phasor data concentrator (PDC) or control center where compressed streaming data are reconstructed. Fig. 4 illustrates

the schematic of an ASBC decoder. The functionalities of individual components are explained below.

The de-multiplexing block is the inverse of the multiplexing block at the encoder. It parses the single bit-stream into subband data streams x_k^Q and x_e^Q sent by the transmitter.

The decompression block reverses the compression block and generates estimated harmonics (in baseband) \hat{y}_k in two steps. First, $x_k^Q[n]$ is up-sampled (interpolated) with zeros (including replacing masked symbols with zeros) to generate sequence $u_k[n]$ that has the same data rate as that of $y_k[n]$. The interpolated sequence $u_k[n]$ is passed through a subband interpolation filter \mathcal{H}^\dagger with impulse response $\hat{h}_k[n]$ to produce an estimate of the baseband representation of the k th harmonic signal $y_k[n]$. The subband interpolation filter may be chosen as the matched-filter $\hat{h}_k[n] = h_k[-n]$ to maximize the signal-to-noise ratio. Other implementations such as windowed low-pass filters can also be used. The decompression of the interharmonic signal follows directly the decompression algorithm used at the encoder.

The final decompression step takes the subband signals $\hat{y}_k[n]$ produce an estimate of the original direct sampled $x[n]$ of $x(t)$ in the encoder:

$$\hat{x}[n] = \sqrt{2}\text{Re}\left(\sum_{k=0}^K \hat{y}_k[n] e^{jk\omega_0 n}\right) + \hat{y}_e[n].$$

V. RATE-DISTORTION CHARACTERISTICS

The standard measure of lossy compression is the rate-distortion curve that highlights the tradeoff between the level of compression and the accuracy of the reconstruction. In general, a well designed compression scheme should have a monotonic rate-distortion curve: the higher the rate of the compressed signal, the lower the distortion.

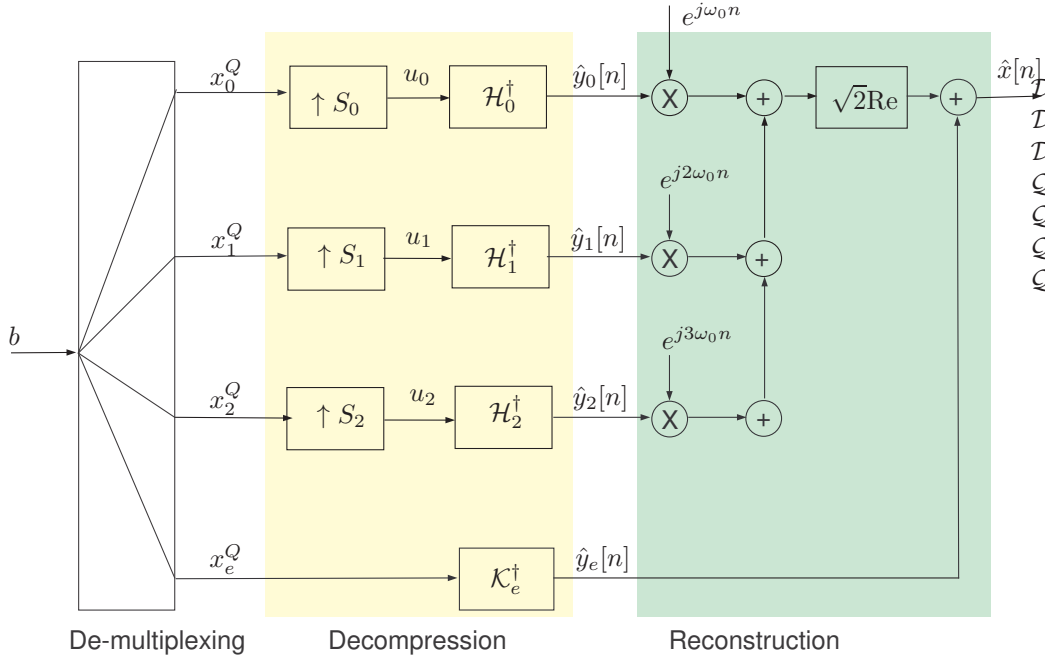


Fig. 4. A three-subband ASBC decoder. Time indices of internal signals (x_i^Q, u_i) are omitted.

In this paper, we adopt the compression ratio and the normalized mean-squared error to characterize the rate-distortion characteristics. Given a compression scheme χ , its *compression ratio* defined by

$$\eta^\chi = \frac{R^{\text{uc}}}{R^\chi},$$

where R^{uc} is the data rate (bits/sec) of the uncompressed signal and R^χ the rate of the compressed stream.

Let $x[n]$ be the original (uncompressed) signal and $\hat{x}^\chi[n]$ the reconstructed signal at the decoder. The *normalized mean-squared error (NMSE)* in (dB) is defined by

$$\begin{aligned} \mathcal{E}^\chi &= 10 \log_{10} \frac{\sum_{n=1}^N |x[n] - \hat{x}^\chi[n]|^2}{\sum_{n=1}^N x^2[n]} \text{ (dB)} \\ &\rightarrow 10 \log_{10} \frac{\mathbb{E}(|x[n] - \hat{x}^\chi[n]|^2)}{\mathbb{E}(|x[n]|^2)} = (\text{SNR}^\chi)^{-1} \end{aligned} \quad (4)$$

where N is the length of the data sequence, and the mean-square convergence of (4) assumes regularity conditions. Note that $\frac{1}{\mathcal{E}^\chi}$ has the interpretation to be the signal-to-reconstruction noise ratio (SNR).

For the application at hand, the data rate of the uncompressed data stream can be measured by

$$R^{\text{uc}} = F_s R_Q \text{ (bits/sec)}$$

where F_s represents the sampling frequency of the measured signal $x(t)$ and R_Q the rate of quantization (bits/sample). The distortion of the uncompressed scheme comes only from

quantization error. For the simple R_Q bits PCM quantization, the NMSE is approximately by

$$\mathcal{E}^{\text{uc}} \approx -6R_Q + 1.25 \text{ (dB)}.$$

See [20, p. 197].

A. Rate-distortion measure of ASBC: ($\eta^{\text{ASBC}}, \mathcal{E}^{\text{ASBC}}$)

We provide a characterization of the compression ratio η^{ASBC} and the NMSE of the reconstruction $\mathcal{E}^{\text{ASBC}}$.

The data rate of the compressed data stream by ASBC is

$$R^{\text{ASBC}} = \sum_{k=0}^K p_k \frac{F_s}{S_k} R_k + p_e F_s R_e \text{ (bits/sec)}, \quad (5)$$

where F_s is the sampling frequency of the uncompressed data, p_k the probability of k th subband being active, R_k the rate (bits/sample) of the quantization in the k th subband, S_k the down-sampling rate of k th subband, p_e the probability that the interharmonic subband is active, and R_e the rate of quantization of the interharmonic subband. The compression ratio of ASBC is given by

$$\eta^{\text{ASBC}} = \frac{R^{\text{uc}}}{R^{\text{ASBC}}} = \left(\sum_{k=0}^K p_k \frac{R_k}{R_Q S_k} + p_e \frac{R_e}{R_Q} \right)^{-1}.$$

If we ignore quantization, ASBC gains via adaptively down-sampling of subband signals based on subband activity. As an example, for the 6kHz sampling of the original signal and

a harmonic subband of 6Hz bandwidth, ASBC achieves the compression ratio 1000 : 1 for that subband.

The NMSE measure $\mathcal{E}^{\text{ASBC}}$ of ASBC depends on how accurately ASBC can detect the activities of harmonic and interharmonic subbands. Assuming all harmonic subbands are active and there is no interharmonics, *i.e.*, $p_e = 0$, we have $\mathcal{E}^{\text{ASBC}} \approx \mathcal{E}^{\text{uc}}$ because ASBC achieves perfect reconstruction of each harmonic signals by the Nyquist sampling theorem. In practice, $\mathcal{E}^{\text{ASBC}} > \mathcal{E}^{\text{uc}}$ when false negative detection occurs or when there is interharmonic signal.

B. Rate-distortion measure of FFT-(k, L) : ($\eta^{\text{FFT}}, \mathcal{E}^{\text{FFT}}$)

A benchmark compression scheme is based on the fast Fourier transform (FFT), herein referred to as FFT-(k, L). It takes a block of L data samples, computes the FFT coefficients, and keeps only the k largest coefficients (corresponding to the positive frequencies) and masks the rest.

The compression ratio of FFT-(k, L) is given by

$$\eta^{\text{FFT}-(k, L)} = \frac{L}{2k}$$

where we ignore the $\log_2 L$ bits needed to encode the frequency locations⁴. The NMSE of FFT-(k, L) is given by

$$\mathcal{E}^{\text{FFT}-(k, L)} = 10 \log \left(1 - \frac{\sum_{i=1}^{2k} |X_{(i)}|^2}{\sum_{i=1}^N |x[i]|^2} \right)$$

where $X_{(i)}$ is the discrete Fourier coefficients with the i th largest magnitude in the L -block FFT.

VI. NUMERICAL RESULTS

We present in this section numerical results in three categories. The first category is a comparison study using a set of synthetic waveforms having characteristics of power system signals. Such tests allow us to evaluate the performance of benchmark techniques under different scenarios of transient events. The second category is the compression of real data obtained by direct sampling of voltage measurements at 6 kHz. This is a case that the signal has significant harmonics and interharmonics. The third category is the compression of compression techniques on streaming of PMU frequency measurements.

The three benchmark techniques compared in this study were (i) FFT described in Sec. V-B, (ii) Multi-resolution discrete wavelet transform (DWT) [16], and (iii) ASBC developed in this paper. All three methods were implemented based on a 0.5-second data block. We measured the performance of compression by the rate-distortion curve by plotting the NMSE (dB) against the compression ratio η . The maximum reconstruction error measure was also used.

Note that the rate-distortion curves typically slope downward: the greater the η^{-1} , the lower the compression ratio (the higher the data rate of the compressed data stream), the lower the reconstruction error.

⁴Note that the factor 2 in the denominator accounts for the fact that FFT coefficients are in general complex and anti-symmetrical for real $x[n]$.

TABLE I
TEST WAVEFORMS

Test cases	Signal waveforms
Normal state: $\sigma_t = 0$	$x_N(t) = \sum_{k=0}^K a_k \cos(2\pi 60(k+1)t + \phi_k)$
Event: $\sigma_t = 1$	$x^{\text{AM}}(t) = (\alpha_0 + \alpha \cos(2\pi \Delta t)) \cos(2\pi 60t + \theta_0)$ $x^{\text{FM}}(t) = \alpha \cos(2\pi 60t + \beta \cos(2\pi \Delta t - \pi) + \theta_0)$ $x^{\text{Chirp}}(t) = \alpha \cos(2\pi(59.5 + \gamma t) + \theta_0)$ $x^{\text{IH}}(t) = \sum_{k=1}^W \alpha_k \cos(2\pi f_k t + \theta_k)$

Signal parameters: σ_t —the switching state, (a_k, ϕ_k) —amplitude and phase angles of harmonics, $(\alpha_k, \beta, \gamma, \theta_k)$ —transient parameters, and f_k —interharmonic frequencies.

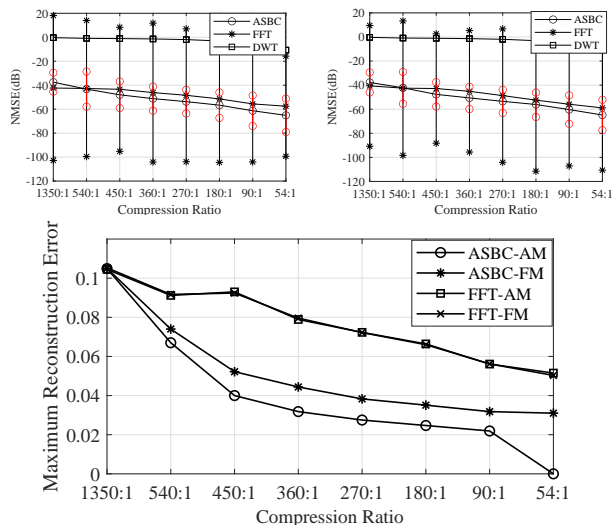


Fig. 5. FM/AM parameters: $\alpha_0 = 1, \lambda = 0.1, \mu = 2$. Top panel NMSE with 95% confidence interval for the AM (Left) and FM (right) events. No high order harmonics and interharmonics. Bottom: the maximum reconstruction error for the FM and AM events.

A. Compression of synthetic waveforms

The purpose of this experiment was to test the performance of compression when the regular sinusoidal waveform was interrupted by episodes of transient events with signals of different characteristics. We focused on four types of event signals shown in Table I. Among the set of waveforms at the event state, the amplitude modulation (AM) and frequency modulation (FM) waveforms were designed according to the requirement on performance under dynamic compliance specified by [4]. The linear chirp waveform was used to simulate the frequency ramping events, and the interharmonic (IH) waveform modeled frequency components that were not multiples of system frequency F_0 .

To simulate transient events, we used a two-state Markov switching model that modulated the signal between the normal state ($\sigma_t = 0$) waveform $x^{\text{Norm}}(t)$ and the event state ($\sigma = 1$) with waveforms chosen from AM, FM, chirp, and IH signals. The Markov switching process was characterized

by state transition rate (λ, μ) where $1/\lambda$ was the expected holding time of the normal state and $1/\mu$ the expected holding time of the event state.

Fig. 5 shows the rate-distortion curve of ASBC, FFT, and DWT techniques for the FM and AM events. The sampling rate of the original signal was at 5400 Hz. As shown in the upper panel, the NMSE of DWT scheme was about 30 to 40 dB higher than those of FFT and ASBC. ASBC had about 4-6 dB gain over FFT for the compression ratio between 540:1 and 54:1 whereas FFT had 3 dB gain at compression ratio of 1350:1. Note that the 95% confidence interval of ASBC was considerably smaller than that of FFT, indicating that the errors of FFT scheme were more dispersed. The same behavior was confirmed by the maximum reconstruction error plot at the lower panel of Fig. 5. DWT, on the other hand, had a much narrower confidence interval (thus not shown on the plot). The main reason that ASBC outperformed FFT was that FFT introduced discontinuities at the boundaries of FFT blocks. In contrast, ASBC encoder did not have discontinuities. This phenomenon was more pronounced for the linear-chirp test cases shown in Fig. 6

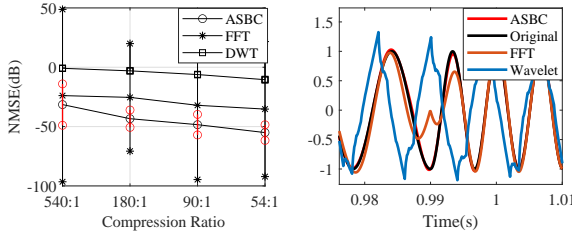


Fig. 6. Left: comparison of rate-distortion curve for linear chirp events. Right: a segment of the original and its reconstruction. $\lambda = 0.1$, $\mu = 1$

Fig. 6 shows the rate-distortion plot for the linear chirp events. The linear chirp signals have a much wider bandwidth and the achievable compression ratio significantly lower than the FM/AM events. The left panel shows the NMSE for the three techniques. Again, DWT was not competitive against FFT and ASBC techniques, and ASBC had considerable gain over FFT in the low compression ratio regime. In particular, ASBC had about 15 dB lower NMSE at the compression ratio of 180:1 and 20 dB lower at the compression ratio of 54:1. The right panel shows the original signal and reconstructed ones in the time domain. Notice the transition of the normal sinusoidal waveform transitioned to a linear chirp at time $t = 0.99$ second. The reconstruction of FFT around $t = 0.99$ showed significantly larger error than that of ASBC.

B. Compression of Direct Voltage Measurements.

We applied ASBC directly to a data set (henceforth referred to as UTK6K) provided the University of Tennessee, Knoxville. The UTK6K data set consisted of 1.8 million voltage measurements sampled at 6KHz. Fig. 7 (Top) shows the power spectrum of the directly sampled data stream,

from which we observed the presence of harmonics and interharmonics. The plot also showed that the energy levels from the 20th to 50th subbands were negligible.

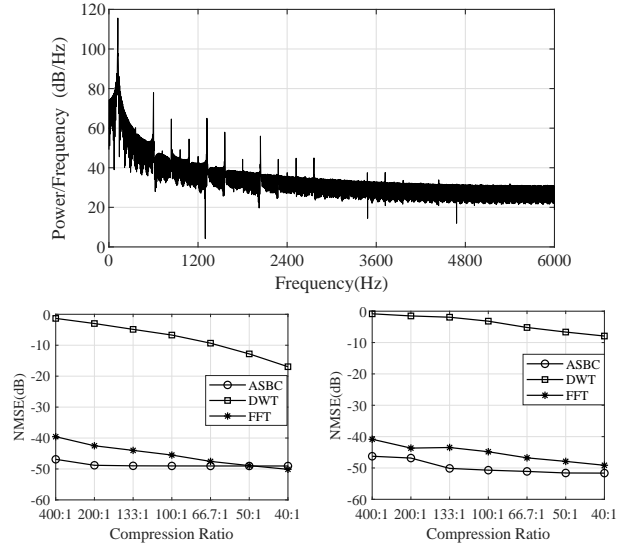


Fig. 7. Top: Power spectrum density of the direct voltage measurements. Bottom left: comparison of rate-distortion curves without interharmonics. Bottom right: comparison with added interharmonics.

ASBC was implemented with 3 Hz bandwidth for all subbands associated with all 50 harmonics, and only the top k subbands that have the highest energy level were compressed and delivered where k was chosen to have required compression ratio. The bottom left panel of Fig. 7 shows the rate-distortion curve of ASBC, FFT and DWT for the compression ratio from 400:1 to 40:1. For this range of compression ratio, DWT was not competitive. ASBC was seen to out-perform FFT in the compression ratio range of 400:1 to 100:1, and the two schemes are comparable for the range of 66.7:1 to 40:1. The reason that FFT-based compression did not perform well was, again, that the block implementation of FFT introduced discontinuities, which caused reconstruction errors. As the compression ratio decreased, more FFT coefficients were preserved, the reconstruction error of FFT improved.

To evaluate the effects of interharmonics, we added additional interharmonic transient events to the original UTK6K dataset in the same way as experiments discussed in Sec. VI-A. The bottom right panel of Fig. 7 shows the rate distortion plot with interharmonics subband activated. An energy detector was used to determine when and whether the interharmonics subband should be activated. Only those harmonics subbands with sufficient energy level were compressed and transmitted. Interharmonics subband, when detected being active by the energy detector, was compressed dynamically to the effective bandwidth ranging from 60 to 120Hz. Comparing with the rate-distortion performance on the bottom left panel, The presence of interharmonics increased NMSE slightly for ASBC at the high compression

ratio. Overall, ASBC consistently performed better than other methods. The standard deviations was small for all three methods, thus the confidence intervals were not shown in the plot.

C. Compression of PMU data

We applied ASBC to a dataset referred to as UTK1.44, which consisted of frequency estimates from the University of Tennessee, Knoxville. The dataset contained two data streams, each with 1,800,000 samples at the rate of 1440 samples/sec. One distinct feature of this dataset was the frequency ramping event between 308.4 and 308.6 seconds as shown in the lower panel of Fig. 8. For this application, the frequency measurements were expected to be centered around 60 (Hz). As a time series, the frequency measurements are close to be constant. Thus only a single subband is needed for ASBC. We varied the subband bandwidth to achieve different compression ratios.

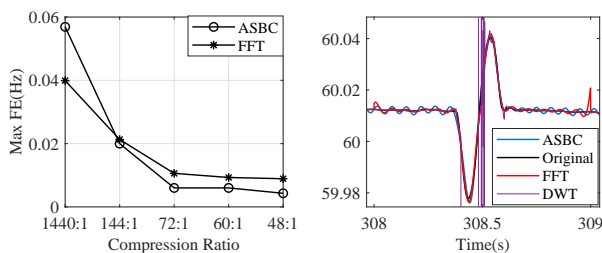


Fig. 8. Maximum FE and time-domain reconstruction

The performance of the three data compression method was evaluated base on the maximum error of the reconstruction of the frequency measurements (Max FE) as defined by the IEEE Standard C37.11 [4] that specified the acceptable performance is to have Max-FE below 0.005 Hz. The left panel of Fig. 8 shows the Max-FE against compression ratio. Max-FE for DWT was always larger than 80, thus is not shown in the plot. In this case, ASBC and FFT appeared to have similar performance along the rate-distortion curve, both having Max-FE below 0.005 for compression ratios lower than 72:1, within which ASBC performed slightly better. The right panel of Fig. 8 showed the time-domain reconstructions at the compression ratio of 48:1. Note that the small spike of reconstruction error of FFT at round $t = 309$ sec caused by, again, the discontinuity of the block implementation of FFT.

VII. CONCLUSION

We have developed an adaptive subband compression (ASBC) technique for the high-fidelity and high-resolution streaming of PMU and POW measurements for wide-area monitoring and control. Different from existing technologies, ASBC decomposes measurements based on the harmonic structure of the signal waveforms and adaptively compresses

individual harmonic components. A prototype implementation of ASBC offers a significantly improved rate-distortion tradeoffs.

REFERENCES

- [1] S. M. Dibaji, A. Annaswamy, A. Chakraborty, and A. Hussain, "Sparse and distributed control of wide-area power systems with large communication delays," in *2018 Annual American Control Conference (ACC)*, June 2018, pp. 3822–3827.
- [2] Y. Liu, "Beyond today's synchrophasor," in *NSF Workshop on Forging Connections between Machine Learning, Data Science, and Power Systems Research*, March 2020, [ONLINE], available (2020/8/20) at <https://sites.google.com/umn.edu/ml-ds4pes/presentations>.
- [3] IEEE, "IEEE standard for interconnection and interoperability of distributed energy resources with associated electric power systems interfaces," *IEEE Std 1547-2018 (Revision of IEEE Std 1547-2003)*, pp. 1–138, April 2018.
- [4] —, "IEEE standard for synchrophasor data transfer for power systems," *IEEE Std C37.118.2-2011 (Revision of IEEE Std C37.118-2005)*, pp. 1–53, Dec 2011.
- [5] M. P. Tcheu et al., "The compression of electric signal waveforms for smart grids: State of the art and future trends," *IEEE Transactions on Smart Grid*, vol. 5, no. 1, pp. 291–302, Jan 2014.
- [6] C. E. Shannon, "A mathematical theory of communication," *Bell Sys. Tech. Journal*, vol. 27, pp. 379–423, 623–656, 1948.
- [7] K. Mehta and B. D. Russell, "Data compression for digital data from power systems disturbances: requirements and technique evaluation," *IEEE Transactions on Power Delivery*, vol. 4, pp. 1683–1688, 1989.
- [8] T. Cover and J. Thomas, *Elements of Information Theory*. John Wiley & Sons, Inc., 1991.
- [9] T. B. Littler and D. J. Morrow, "Wavelets for the analysis and compression of power system disturbances," *IEEE Transactions on Power Delivery*, vol. 14, no. 2, pp. 358–364, April 1999.
- [10] S. Santoso, E. J. Powers, and W. M. Grady, "Power quality disturbance data compression using wavelet transform methods," *IEEE Transactions on Power Delivery*, vol. 12, no. 3, pp. 1250–1257, July 1997.
- [11] A. M. Gaouda, M. M. A. Salama, M. R. Sultan, and A. Y. Chikhani, "Application of multiresolution signal decomposition for monitoring short-duration variations in distribution systems," *IEEE Transactions on Power Delivery*, vol. 15, no. 2, pp. 478–485, April 2000.
- [12] S. Santoso, E. J. Powers, W. M. Grady, and A. C. Parsons, "Power quality disturbance waveform recognition using wavelet-based neural classifier. i. theoretical foundation," *IEEE Transactions on Power Delivery*, vol. 15, no. 1, pp. 222–228, Jan 2000.
- [13] P. K. Dash, B. K. Panigrahi, D. K. Sahoo, and G. Panda, "Power quality disturbance data compression, detection, and classification using integrated spline wavelet and s-transform," *IEEE Transactions on Power Delivery*, vol. 18, no. 2, pp. 595–600, April 2003.
- [14] N. Tse et al., "Real-time power-quality monitoring with hybrid sinusoidal and lifting wavelet compression algorithm," *IEEE Transactions on Power Delivery*, vol. 27, no. 4, pp. 1718–1726, Oct 2012.
- [15] S. Meher, A. Pradhan, and G. Panda, "An integrated data compression scheme for power quality events using spline wavelet and neural network," *Electric Power Systems Research*, vol. 69, pp. 213–220, 2004.
- [16] J. Ning, J. Wang, W. Gao, and C. Liu, "A wavelet-based data compression technique for smart grid," *IEEE Transactions on Smart Grid*, vol. 2, no. 1, pp. 212–218, March 2011.
- [17] W. R. A. Ibrahim and M. M. Morcos, "Novel data compression technique for power waveforms using adaptive fuzzy logic," *IEEE Transactions on Power Delivery*, vol. 20, no. 3, pp. 2136–2143, 2005.
- [18] Y. Ge, A. J. Flueck, D. Kim, J. Ahn, J. Lee, and D. Kwon, "Power system real-time event detection and associated data archival reduction based on synchrophasors," *IEEE Transactions on Smart Grid*, vol. 6, no. 4, pp. 2088–2097, July 2015.
- [19] A. Testa et al., "Interharmonics: Theory and modeling," *IEEE Transactions on Power Delivery*, vol. 22, no. 4, pp. 2335–2348, 2007.
- [20] A. V. Oppenheim and R. W. Schaffer, *Discrete-Time Signal Processing*, 2nd ed. USA: Prentice Hall Press, 1999.